Available online at www.sciencedirect.com
ScienceDirect
Continental Shelf Research 26 (2006) 2629–2644
CONTINENTAL SHELF RESEARCH
www.elsevier.com/locate/csr

Studies on turbulent diffusion processes and evaluation of diffusivity values from hydrodynamic observations in Corpus Christi Bay

Temitope O. Ojo, James S. Bonner*, Cheryl Page

Civil Engineering Department, Texas A & M University, College Station, TX 77843-3136, USA

Received 7 October 2004; received in revised form 15 June 2006; accepted 18 August 2006
Available online 27 October 2006

Abstract

The physical process of dispersion which can be attributed to turbulence (*turbulent diffusion*) or shear (*shear-augmented diffusion*) within the flow field is very important as it ultimately governs the distribution of constituents of interest within the environment. A series of diffusion experiments were conducted in Corpus Christi Bay, TX with the purpose of characterizing turbulent diffusion through dispersion coefficients or turbulent diffusivity, $\boldsymbol{K_i}$ ($i = x, y, z$) dependent on the degree of randomness or turbulence intensity, I.

Measured with a boat-mounted acoustic doppler current profiler (ADCP), the Eulerian velocity time-series of fluid particles in random motion, u_i was used in the evaluation of the Eulerian time-scale of turbulence, $\boldsymbol{T^E}$ based on the velocity correlation function, $\boldsymbol{R^E}$ with $\boldsymbol{T^E}$ being related to the Lagrangian time-scale $\boldsymbol{T^L}$ through a scaling parameter, $\beta(= T^L/T^E)$. Surface currents were obtained with high frequency (HF) Radar equipment deployed over the study area from which the horizontal velocity gradients were determined.

Within the spatial scale of the experiment ($\sim$1000 m), the observed low horizontal gradients ($\sim 10^{-4}\,s^{-1}$) allowed for the generation of velocity time-series from an ADCP mounted on a moving platform. A numerical scheme for evaluating turbulent diffusivity values $\left(K_i = \beta\overline{u_i'^2}T^E\right)$ was developed on the basis of Eulerian current measurements and calibrated through the statistics of an evolving dye patch for the scaling parameter β which in this scheme was found to be in the range 1–3.

Keywords: Autocorrelation; Diffusion coefficients; Eddy diffusivity; Mixing processes; Turbulence; Turbulent diffusion; USA; Gulf of Mexico; Texas; Corpus Christi Bay

1. Introduction

Diffusion processes in surface waters are important as they govern the overall concentration distribution of constituents (salinity, phytoplankton, sediments, temperature, heat etc.) within the water body. A concentration profile of these constituents can be developed using numerical models that often require parameterization, which capture the physical phenomena that lead to dispersion, and are collectively termed dispersion

*Corresponding author. Tel.: +1 979 218 6438.
E-mail address: bonner@tamu.edu (J.S. Bonner).

0278-4343/$ - see front matter © 2006 Published by Elsevier Ltd.
doi:10.1016/j.csr.2006.08.007

coefficients. The coefficients may be determined through:

(i) The evaluation of the temporal variation of the currents;
(ii) The evaluation of the spatial variation of the velocity field;
(iii) The evaluation of the first and second moments of concentration distribution of a constituent and;
(iv) Inverse problem based on the advection–diffusion equation.

The first two methods are based on Taylor's work on the analysis of fluid flow through pipes (Taylor, 1954) and extended to other fluid flow regimes by Elder in his work on flow through open channels (Elder, 1958). Typically, the third method (and the fourth being a variant of the third) is used in surface waters whereby a conservative tracer is tracked through time and space. There have been very few applications of the first two methods in the open waters typical of bays, estuaries and the coastal ocean but an example of the adaptation of the first to the open ocean was in a study conducted at the 106-Mile ocean disposal site (Paul et al., 1989). In Paul's study, long-term current meter readings were used in estimation of the dispersion of waste sludge under high- and low-turbulence conditions on a spatial scale of the order of 100 km and temporal scales of the order of 100 days.

By obtaining the probability distribution of the velocity measurements along independent coordinate axes, the variance–covariance property of the distribution was used based on the assumption that the averaged mass–distribution of a constituent would be described as a multiple of the velocity distribution. In related work (O'Connor et al., 1985) the turbulent process in open waters was categorized using three broad spatial-temporal classifications viz. small, intermediate and large:

Small scale	Intermediate scale	Large scale
Temporal scale <24 h, spatial scale between 0 and 10 km	Temporal scale between 1 and 100 days, spatial scale between 10 and 300 km	Temporal scale >100 days, encompassing the ocean basin

This study is restricted to small-scale processes where tidal and inertial motions are considered advective and the velocity fluctuations about the tidal mean are responsible for diffusion or turbulent mixing. This is in contrast to intermediate and large-scale processes where the tidal and inertial currents will be considered diffusive. This scale dependence of the turbulent diffusion process was compiled into a set of oceanic diffusion diagrams (Okubo, 1971) based on data obtained for the open ocean, which may not find much applicability within the coastal and nearshore environments. In light of this, a similar set of diffusion diagrams are needed specifically for the coastal ocean but data on the diffusive process within these areas will have to be developed.

This study is aimed at extending Taylor's work into environmental field applications with emphasis on the nearshore environment. The authors are aware that this is the first attempt to directly evaluate turbulent diffusivities in shallow waters within a Eulerian framework using measurements taken with an acoustic doppler current profiler (ADCP). It forms part of ongoing research efforts aimed at developing an integrated system for environmental monitoring within Corpus Christi Bay in particular and the Texas Gulf of Mexico region in general. The overall objective is to be able to completely characterize the area in terms of physical, bio-chemical, environmental and oceanographic parameters using current state-of-the-art in in-situ sensors and remote sensing. Currently, a system of high frequency (HF) radar has been deployed around the Texas Gulf of Mexico covering areas around Corpus Christi Bay, Matagorda Bay and Galveston Bay providing real-time surface current measurements (Kelly et al., 2004) and efforts are underway to expand the capability for response to episodic events (Kelly et al., 2002; Ojo and Bonner, 2002; Ojo et al., 2003a).

A system of fixed and mobile platforms complement the radar system using in-situ instrumentation, which provide environmental measurements from within the study area, variables that can be assimilated into numerical schemes operating in a predictive mode (Ojo et al., 2003b, c) within the framework of environmental and oceanographic assessments. The integrated scheme combining these real-time measurements with numerical transport modeling (Sterling et al., 2004a, b) needs to be effectively characterized and parameterized (Ernest

et al., 1991; Lee et al., 2000) in order to be fully operational.

Turbulent diffusion in surface waters being analogous to molecular diffusion as a stochastic process (Taylor, 1920), a coefficient of turbulent diffusivity or eddy diffusivity can be developed which will be found to be several orders of magnitude higher than molecular diffusivity values. In addition, constituent transport in the turbulent regime can be modeled as Fickian diffusion with constant coefficients, conditionally dependent on a Lagrangian time scale of turbulence, T^L derived from the velocity autocorrelation function, $R(\tau)$ as presented in the classical work of Taylor. The difficulty of course lies in obtaining Lagrangian (moving reference frame) measurements of fluid particles since field measurements of current in surface waters are usually Eulerian (fixed reference frame). Through a series of dye experiments conducted in the Baltic (Schott, 1978) with a set of vector-averaging current meters (VACM), previous work in atmospheric dispersion (Hay and Pasquill, 1959) was extended to the oceanographic field. Both of these studies investigated the relationship between the Lagrangian and Eulerian statistics through a scaling of the time axis for the velocity autocorrelation function through an empirical coefficient β that serves the purpose of preserving the shape of the autocorrelation function. Ranging in value between 1 and 4, a value of ~4 was found to give adequate results for meteorological applications and no specific prescription has been found in the literature for oceanographic applications.

Bowden–Fairbairn deployed two fast response current meters that were capable of responding to fluctuations with a period of ~2 s (Bowden and Fairbairn, 1952) in the Mersey Estuary (Great Britain) from which they were able to directly obtain the values of $R(\tau)$. Bowden and Howe used the same approach within the same study area but using an electromagnetic flowmeter that could sample fluctuations with periods ~1 s (Bowden and Howe, 1963) comparing with the VACM used by Schott which averaged currents over a period of 112 s. Our approach is similar to that used by Bowden and Howe (1963) employing a fast response current profiler and direct numerical analysis of the velocity time series for the evaluation of $R(\tau)$ and T^L. The current profiler we employed was capable of sampling with a period ~0.5 s.

In this study, there are three main research objectives. The first deals with analysis of the spatial and temporal characteristics of observed 3D velocity field within Corpus Christi Bay. Errors associated with the development of velocity time series from a moving platform are examined given the horizontal current shear. The second deals with evaluation of the time scale of the turbulent process and subsequently developing a numerical scheme for estimation of turbulent diffusivity from observations of the 3D current profile within an Eulerian framework. The third and final objective calibrates the numerical scheme directly against diffusivity values obtained from the concentration profile of a diffusing dye patch. A relationship between the Lagrangian and Eulerian frameworks is established through the resulting scaling parameter β which is also the ratio between the Lagrangian and Eulerian timescales.

This work is important as it provides a parameterization scheme for the diffusive component of constituent transport that is applicable irrespective of meteorological, oceanographic and geomorphologic regimes and without recourse to expensive and time-consuming tracer experiments. Furthermore, it extends the application of current profiling instruments beyond the realm of oceanographic measurements of velocity into the area of environmental monitoring.

1.1. Turbulent diffusivity

The statistical process of diffusion relates to a diffusion coefficient, K given by

$$K = \overline{u'^2} \int_0^t R(\tau)\mathrm{d}\tau, \tag{1}$$

$$R(\tau) = \frac{\overline{u'(t)u'(t+\tau)}}{\overline{u'(t)^2}},$$

where τ is a lag time between successive observations of the velocity, u of a fluid particle and $\overline{u'^2}$ is the mean-square of the velocity fluctuation of fluid particles in random motion which relates to the degree of randomness or turbulence intensity. The integral of the Lagrangian correlation coefficient, R is the Lagrangian timescale of turbulent diffusion, T^L and for times when $\tau \gg T^L$, the diffusing cloud will grow at a constant rate. The timescale, T^L is regarded as the 'persistence time' of the particle velocities after which the particles have lost all memory of their initial velocities. With respect to a set of coordinate axes and in terms of the respective

time scale, T_i^L,

$$\begin{aligned} K_i &= \overline{u_i'^2} T_i^L, \\ T_i^L &= \int_0^t R_i(\tau)\,\mathrm{d}\tau, \\ u_i(t) &= \overline{u_i(t)} + u_i'(t), \end{aligned} \tag{2}$$

for $i = x, y, z$ corresponding to the coordinate axes. The quantity $u_i'(t)$is the ith component measured at time t, of the Lagrangian velocity fluctuation around a supposedly steady mean velocity, $\overline{u_i(t)}$ of a tagged particle experiencing turbulence in a fluid, and τ [0 ∞] is a lag time for the ensemble of velocity measurements. The ratio of the rms velocity fluctuation to the mean velocity is the turbulence intensity $I(=\sqrt{\overline{u_i'^2}}/\overline{u_i})$ the overbar indicating an ensemble mean of realizations u_i of the velocity components over a period of time. Several models have been proposed for R_i by researchers to describe specific flow regimes (Frenkiel, 1953) including the simple exponential form used by Taylor in his classical work on turbulence. The integral in Eq. (2) leads to the evaluation of K_i if the mean square of the velocity fluctuation, $\overline{u_i'^2}$ is known. In oscillating flows commonly experienced in tidal or wind-driven bays and estuaries, $\overline{u_i'^2}$ can be evaluated using a running average over a suitably large number of ensembles. Certain requirements for $R_i(\tau)$ are imperative in order to find analytical forms for K_i but in complex flow regimes typical of bays and estuaries within temporal scales of the order of minutes and spatial scales of the order of a few thousand meters, the difficulty lies with finding the Lagrangian values in Eq. (2) from the Eulerian statistics that current meter measurements would typically return.

As mentioned earlier, the work of Hay and Pasquill (1959) allows for an expression equivalent to Eq. (2) within an Eulerian framework as follows:

$$\begin{aligned} & K_i = \beta\overline{u_i'^2} \int_0^t R_i(\beta\tau)\,\mathrm{d}\tau, \\ \text{from which} \quad & T_i^E = \int_0^t R_i(\beta\tau)\,\mathrm{d}\tau, \\ & K_i = \beta\overline{u_i'^2} T_i^E, \end{aligned} \tag{3}$$

where T_i^E is the Eulerian timescale derived from the autocorrelation function of the velocity time-series taken from current profiler measurements and $\beta = T^L/T^E = f(I)$, the scaling parameter is the ratio between the timescales is a function of the turbulence intensity (Hanna, 1981). Given the rms velocity fluctuations, K_i can be determined from Eq. (3). Intuitively, we expect $\beta > 1$ and the objective of this study is to determine its value and subsequently develop an expression for K_i by calibrating against the concentration profile of a conservative dye tracer. The validity of this approach is predicated on Taylor's frozen turbulence (Taylor, 1938) hypothesis. Provided the turbulent fluctuations u_i' are small relative to the mean flow velocity $\bar{u}_i$, the turbulent flow pattern being advected along by the mean flow and basically remaining unchanged. Lagrangian velocity fluctuations for practical purposes can therefore be replaced by the Eulerian values derived from current meter measurements.

1.2. Scale of turbulence

Noting that linear growth is a necessary (but not sufficient) condition for Eq. (2) to be applicable within the context of the governing equations of transport (Fischer et al., 1979) an integral length scale l_i is defined as follows:

$$l_i^2 = \overline{u_i'^2} T_i^{L^2} = \beta\overline{u_i'^2} T_i^{E^2}. \tag{4}$$

This length scale, l_i is the distance that a fluid particle must traverse before it loses memory of its initial velocity and the expression in Eq. (4) establishes the scale-dependence for turbulent diffusion. The process of turbulent diffusion can therefore be characterized by the length scale, l_i that depends on the characteristic velocity (root mean square of the velocity fluctuation, $\sqrt{\overline{u_i'^2}}$) and the time-scale T_i^L which in turn depends on the asymptotic property of the velocity autocorrelation function.

For $K_i =$ constant

$$\sigma_i^2 = 2\overline{u_i'^2} T_i^{L^2} = 2l_i^2. \tag{5}$$

If L_i^2 represents the size of the diffusing cloud of particles along a particular coordinate axis, then the turbulent diffusion process can be modeled as Fickian diffusion with a constant diffusivity, K_i in the regime where the cloud size is much larger than the length scale of the turbulence i.e.:

$$L_i^2 \gg 2l_i^2. \tag{6}$$

2. Methods and materials

The study was conducted as part of a series of dye-tracer experiments conducted within Corpus

Table 1
Summary of experimental and meteorological conditions

Id	Location	Date	Time (UTC)	Tide	Wind
0828_1	2747.937 N 9721.451W	Aug. 28, '03	15:44	High water, ebb	7 kn, SE
0828_2	2743.571N 9718.297W	Aug. 28, '03	21:20		14 kn, SE
1007	2747.937N 9721.451W	Oct. 07, '03	14:34	High water, flood	4–12 kn, NE

Christi Bay through the summer and winter of 2003. The analyses given in the preceding sections were applied to Corpus Christi Bay for the characterization of the turbulent diffusion process using the velocity autocorrelation derived from 3D current measurements. Summary of the three studies conducted are given below. For reference purposes identification numbers have been assigned to each study. Two studies were conducted on August 28, 2003 at two different locations and at different times within the tidal cycle. A third study was conducted on October 7, 2003 at the first location but at a time within the tidal cycle different from the time of the first study conducted at that location. This experimental design was for the purpose of elucidating information relating to the hypothesis on spatial-temporal variability of diffusivity values due to the coupling between meteorological conditions and oceanographic forcing within the study area. Table 1 below gives a summary of the study sites, experimental and meteorological conditions.

2.1. Site description

The site where the experiments were conducted is located within Corpus Christi Bay which is in the Texas Gulf of Mexico about 200 miles south west of Houston, TX (Fig. 1). Being part of a system of bays that has Corpus Christi Bay as the main bay, there are four embayments connected within the system namely Oso Bay in the southwest, Nueces Bay in the northwest, Upper Laguna Madre in the south and Redfish Bay in the north–east. A shipping channel that is ~15 m deep runs east to west along the northernmost half of the bay and an intracoastal waterway runs north to south. Corpus Christi Bay is bounded on the east by Mustang and North Padre Islands and on the west by the city of Corpus Christi.

The deepest of the four, it has relatively uniform bathymetry throughout (~3 m) with a correspondingly low tidal range (± 0.5 m) as is characteristic of most of the bays in Texas. The bay is approximately 500 km^2 with the channel opening into the Gulf at the Northeastern end through Aransas Pass as the main form of exchange with the Gulf system and under the influence of the tides, the residual currents are therefore predominantly along the east–west coordinate axis with a counterclockwise circulation pattern along the shoreline. Being in a semi-arid location with freshwater inflow from Nueces River and Oso Creek, the system with a drainage area of ~49,700 km^2 receives a daily average freshwater flow of ~34 m^3/s and has an average salinity of 22 psu which can be as high as 33 psu. This bay, which can be classified as wind-driven is predominantly under the influence of winds blowing from a southeasterly direction year round while winds blowing from a northerly direction are sometimes experienced during the winter months.

2.2. Instrumentation and data acquisition

This section describes the instrumentation used during the experiments. In obtaining the 3D current profiles a fast response 1200 kHz broadband workhorse Acoustic Doppler Current Profiler, ADCP (RD Instruments, Inc., San Diego, CA, USA) installed on a rigid mount on the bow of a 10 m small-watercraft was used. The ADCP is equipped with bottom-tracking capability which allowed for absolute current measurements to be obtained from a moving instrument platform. The built-in algorithm takes into account the velocity of the moving platform during the data acquisition process. With the instrument sampling rate set at 2.5 Hz, current profiles were obtained within a 300–500 m radius dictated by the spatial extent of a dye tracer patch which was simultaneously tracked by a fluorometer

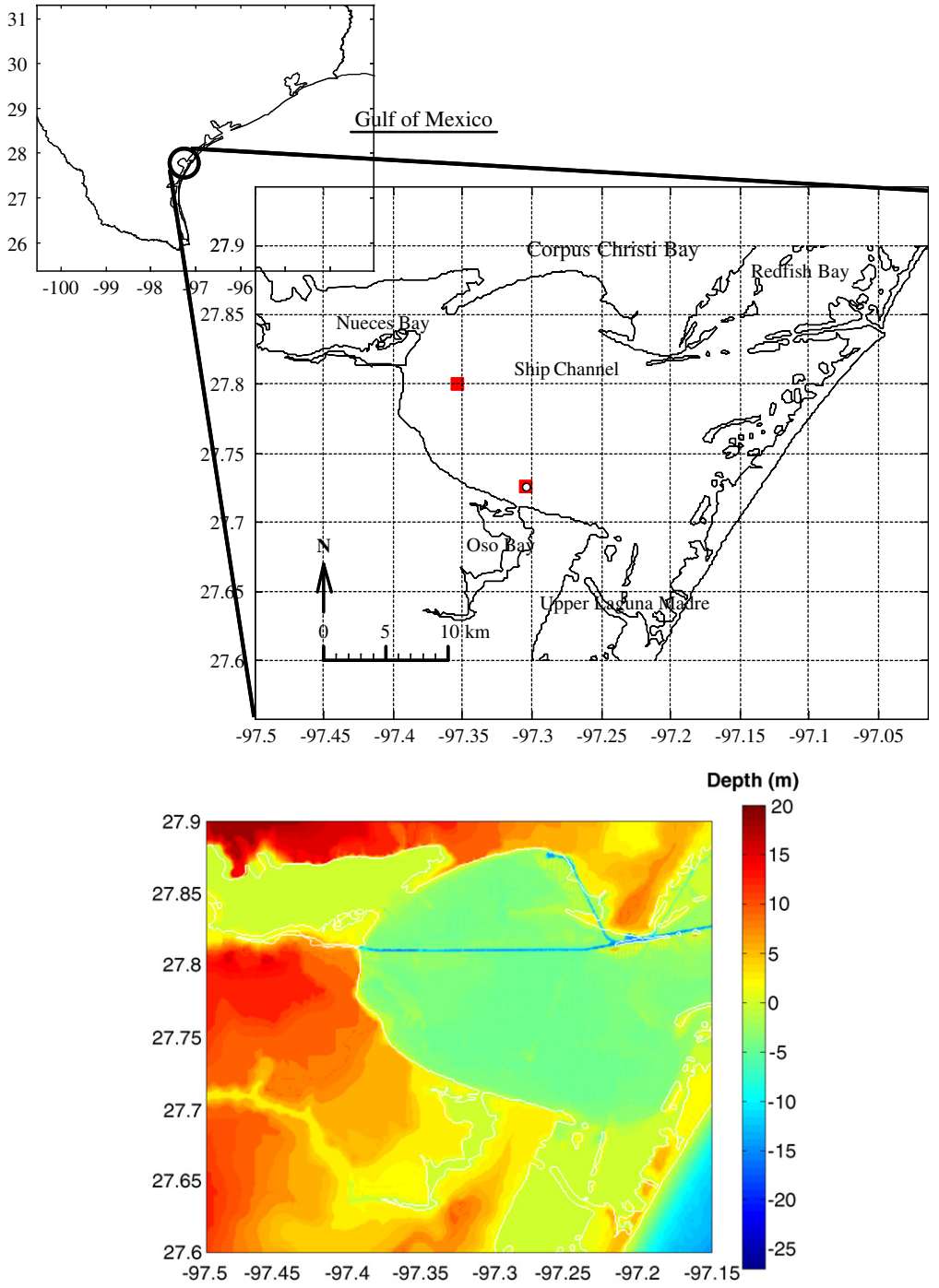

Fig. 1. Top; map of Corpus Christi Bay in the Texas Gulf of Mexico. Approximate location for each study is indicated (■—Study 0828_1 and 1007; ◘ – –Study 0820_2). Bottom; bathymetry of the study area.

mounted on an undulating tow-body. Velocity time series were generated over a period between 120 and 150 min. Additional instrumentation mounted on the tow-body comprised of a SAFIRE multi-spectral fluorometer (WET Labs, Inc., Philomath, OR, USA) for obtaining the concentration distribution of the dye, a CTD (conductivity-temperature-depth) sensor for basic water parameters (Sea-Bird Electronics, Inc., Bellevue, WA, USA), and a LISST-100 (Laser In-Situ Scattering and Transmissometry, type 100) particle size analyzer for particle size distribution measurements (Sequoia Scientific, Inc., Bellevue, WA, USA).

Data logging was carried out on-board the craft with an integrated data acquisition (DAQ) computer incorporating a GPS unit. The profile was well localized both temporally and spatially enough to filter out horizontal variations in current structure and the effects of tides. Surface currents and horizontal shear were obtained from HF Radar (Seasonde^{TM} by CODAR Ocean Sensors, Inc., Mountain View, CA) operated as part of our coastal environmental field facility and permanently deployed in Corpus Christi Bay. It operates on the principle of Bragg Scattering of HF electromagnetic waves incident on surface waves (Barrick et al., 1977). The Doppler shift between transmitted and returning waves provides a measure of the speed of the surface wave with the transmitted and reflected waves also providing a means of georeferencing the resulting currents over the entire spatial domain. The Seasonde has a spatial resolution of about 1 km with a range of 50–70 km allowing for horizontal surface current mapping over the domain of observation.

2.3. Data analysis

In this section, analysis of the spatial and temporal characteristics of the current field and the evaluation of errors that may result from the development of a velocity time series using an ADCP mounted on a moving platform is described.

2.3.1. Velocity time series generation from spatial series obtained from a moving platform

Suppose the first measurement was taken at time t_0 at position P_1 and given a uniform velocity gradient $S(S = \frac{\delta u}{\delta x})$ within the sampling area (Fig. 2).

At time t_1,

$$u_{P_2} = u_{P_1} + S \cdot \Delta x_1.$$

At time t_2,

$$u_{P_3} = u_{P_1} + S\,\Delta x_1 + S\,\Delta x_2.$$

At time t_3,

$$u_{P_4} = u_{P_1} + S\,\Delta x_1 + S\,\Delta x_2 + S\,\Delta x_3.$$

At time t_{n-1},

$$u_{P_n} = u_{P_1} + S(\Delta x_1 + \Delta x_2 + \ldots + \Delta x_{n-1}), \tag{7}$$

$$u_{P_n} = u_{P_1} + S\sum_{1}^{n-1} \Delta x_j, \tag{8}$$

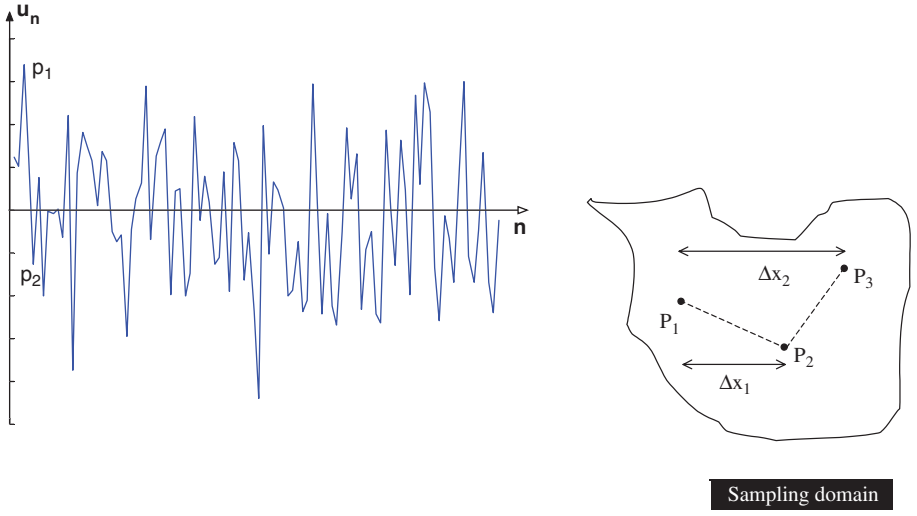

Fig. 2. Left, spatial series of current measurements generated from ADCP mounted on a moving platform; right, illustration of sampling scheme used for current measurements.

Δx_j being the separation between successive sampling points within the domain, u_{P_1} and u_{P_n} are the measurements taken at the respective points, and $t_{n-1}(=nT_s)$, represents the time at which the nth sample was obtained given that T_s is the instrument dependent sample period. Eq. (8) could be written as follows:

$$u_{P_1} = u_{P_n} + \vartheta, \tag{9}$$

where $\vartheta(=S\sum_1^{n-1}\Delta x_j)$ is an error term associated with the sampling scheme and derives from the spatial displacement of the instrument platform relative to point P_1. Hence, at sample point P_1 the time series of velocity is given by the spatial series of measurements that includes an error term additive with the instrument error. Eq. (9) is rewritten for point P_1 as a time series dependent on ADCP measurements (u_{adcp}) as follows:

$$u(t) = u_{adcp} + \vartheta. \tag{10}$$

Let $\Delta x_{n-1} = X_N$ (X_N being the position of sample point P_n in relative coordinates to point P_1, $N = 0, 1, \ldots, n-1$) then,

$$\sum_1^{n-1}\Delta x_j = \sum_0^N X_N = n\overline{X}, \tag{11}$$

$\overline{X}$ is the average displacement of the instrument platform relative to P_1 after n samples. Eq. (10) then becomes:

$$u(t) = u_{adcp} + nS\overline{X}. \tag{12}$$

For transects made up of monotonically increasing set of sampling points, $\overline{X} = X_N/2 = \alpha(n-1)T_s/2$ (α being the travel speed of the moving platform). The time series representation from the spatial series would therefore appear to have an associated error increasing as the square of the number of samples with the error given by:

$$\vartheta = \alpha n(n-1)ST_s/2. \tag{13}$$

By creating a running average of the n samples, the time series at point P_1 becomes

$$u(t) = \overline{u}_{adcp} + S\overline{X}, \tag{14}$$

and the associated error is given by

$$\vartheta = \alpha(n-1)ST_s/2, \tag{15}$$

exhibiting a linear dependence on the number of samples.

The horizontal shear structure was obtained from the velocity gradients using the surface current measurements from HF radar. The currents were resolved into components along each of the x,y-coordinate axis following which the shear structure was determined. The resulting shear structure was subsequently used in Eqs. (13) and (15) along with the velocity series from ADCP to evaluate the error associated with generating velocity time series from a moving platform. The ADCP collects bottom-tracking data simultaneous with the current measurements and this was used in compensating for the motion of the instrument platform as well as subsequent referencing to geographic coordinates.

Data post-processing and analysis were performed with the signal processing toolbox in MATLAB® and a set of routines that were developed in our laboratory. To ensure data quality, spectral analysis was subsequently performed on the velocity time-series using Welch periodogram method to obtain the frequency signature of the ADCP measurements. Following this, a low-pass filter was applied to the velocity signal, the size of the filter determined based upon the observed frequency spectrum. Application of the filter serves the purpose of isolating within the signal, the current fluctuations due to turbulence.

2.4. Eulerian timescale of turbulence and turbulent diffusivity: algorithmic aspects

The generation of velocity autocorrelation, and subsequently the evaluation of turbulent diffusivity using the velocity history of fluid elements are described. For each coordinate axis, the result was an $N \times 30$ matrix of velocities in 30 equally spaced vertical bins through the water column with N, the size of the samples dependent on the duration of the exercise and instrument sampling rate. These were numerically analyzed using the cross-correlation function in the signal processing toolbox with different values of lag τ (in seconds) to obtain the velocity autocorrelation $R_i(\tau)$ in three absolute coordinate axes x, y, z, respectively. The $R_i(\tau)$ values were then used in the numerical evaluation of T_i^E, the Eulerian timescale. For the direct calibration of the algorithm in Eq. (3), turbulent diffusivity values, K_i ($i = x, y$) obtained from the concentration profile of the dye-patch were combined with T_i^E leading to the determination of β.

3. Results

From the three studies, velocity time-series measurements were obtained during each exercise

along with fluorescence measurements providing information and statistics on the evolving dye patch. Evaluation of Eulerian timescale of diffusion, T_i^E from direct observations of the 3D currents field was performed as described in the preceding section. From the obtained fluorescence measurements, the diffusivity K_i was estimated and subsequently the numerical scheme presented in Section 1.1 was calibrated against K_i for the scaling coefficient β in Eq. (3).

3.1. Velocity time series generated from a moving platform—error analysis

Within the sampling domain the horizontal velocity gradient, S were derived from data obtained through surface current mapping using HF radar deployed over the study area by our research group. The evaluated maximum value of S was $\sim 6 \times 10^{-4}\,s^{-1}$ occurring in the direction of the x-coordinate axis and these gradients are represented in the contour plot of Fig. 3. This plot was derived for the instance when the gradients were at a maximum. As would be expected for surface waters, these gradients are relatively low with the highest values occurring around the shoreline and around regions of high flow.

Given transects made up of $n = 1$–100 samples with $T_s = 0.39\,s$, and $\alpha = 2.2\,m/s$, and using the maximum value of S the error associated with the sampling scheme will have the values represented in Fig. 4. From the foregoing analyses for a monotonically increasing transect set although averaging

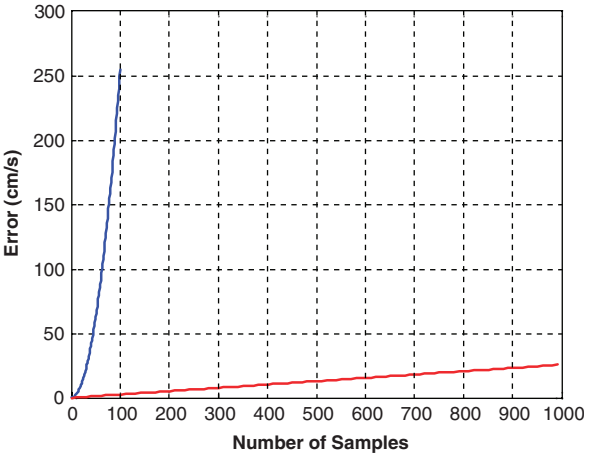

Fig. 4. Errors resulting from velocity time series generated from spatial series evaluated against number of samples in series. The error increases as the square of number of samples for monotically increasing transect design while the relationship is linear for a normally distributed transects.

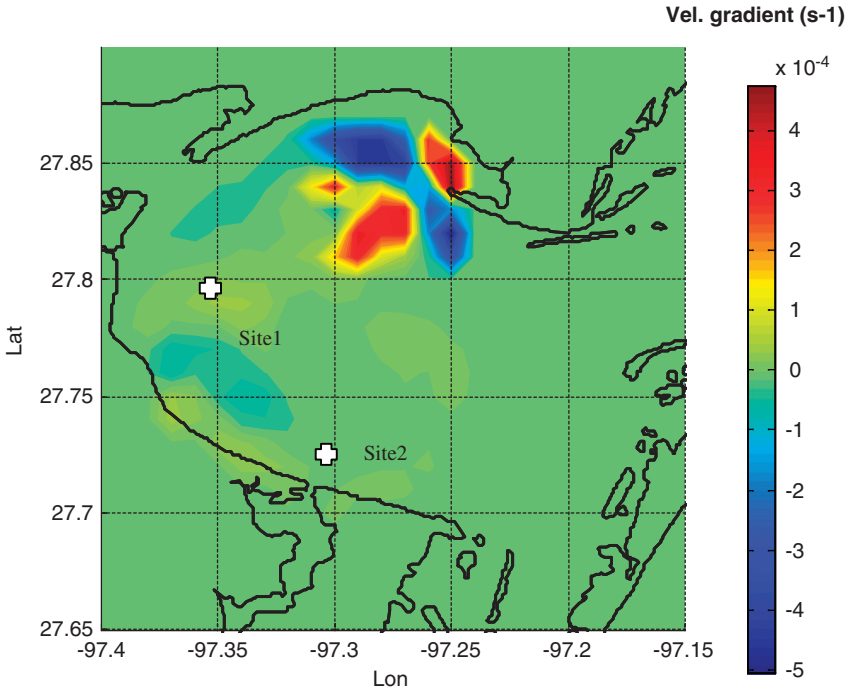

Fig. 3. Horizontal velocity gradients from surface current mapping of the study area.

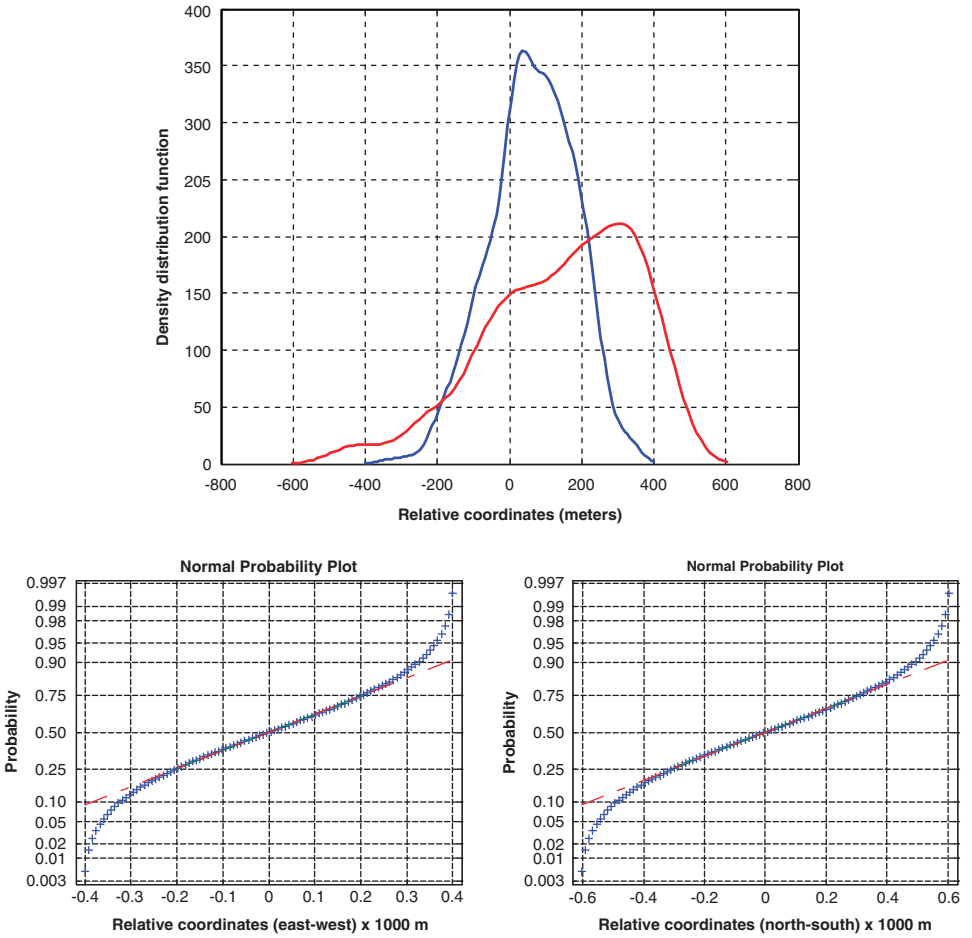

Fig. 5. Top panel: distribution of sampling points in relative coordinates in both east–west (blue) and north–south (red) directions. Bottom: normal probability plot. Left is for east–west and right is for the north–south distribution of (relative coordinates) of the sampling points plotted in blue. The red line is the straight line plot from the ideal normal distribution.

reduces the error significantly, it appears that there can still an unacceptable amount of error in the resultant time series of velocities generated from a moving platform.

For instance, averaging over 1000 samples produces an error of ~25 cm/s while averaging over 100 samples would produce an error of ~2.5 cm/s, a 10-fold reduction. Hence, for these types of transect design, the number of samples would have to be kept small enough to achieve acceptable error levels.

A different type of transect design which was used in this study not made up of monotonically increasing sample points, but of a normally distributed set of points is examined. The probability plots for this (typical) distribution of sampling points within the domain (Fig. 5) reveals the characteristics of the distribution in comparison with the plot (straight line in the figure) from an ideal normal distribution. As seen from the plot, the distribution exhibits linearity between the first and third quartiles indicating that the distribution is indeed normal. The mean (50th percentile) of the sampling points (in relative coordinates) $\overline{X} = 0$ cm and the standard deviation falls within the range 250–350 m.

The normality exhibited by the distribution is helped largely by the large number of samples taken. In generating the time series, one may be tempted to then apply Eq. (12) directly since the zero mean $\overline{X}$ effectively eliminates any sampling error. Eq. (14), which is a running average of the spatial series of velocities, however, allows for using fewer number of sample points and is the preferred method for error reduction as there is no direct dependence on the number of samples when compared to Eq. (12). There is of course an indirect

dependence on the number of samples even with the application of Eq. (14) noting that fewer sample points imply a departure from a normal distribution. It can be argued though that $\overline{X}$ would still be small enough (~0 cm) such that in combination with the low value of the horizontal gradient S therefore, effectively eliminates the sampling error.

It is imperative to note that filtering the spatial series eliminates instrument errors as well but the number of samples required for the running average and hence the filter size is increased to accommodate the additional error inherent in the sampling scheme. For comparison, whereas 10 samples may have been adequate to reduce instrument error by one-third, this number of samples will not be sufficient to produce a distribution that approximates a normal distribution. Increasing this sample size to 100 would produce a better approximation resulting in a 10-fold reduction in instrument error while at the same time reducing the error due to the sampling scheme.

A time series can therefore be produced from a spatial series by careful design of the sampling transects and subsequent application of a suitable filter to the spatial series. The transect should not be composed of monotonically increasing sampling points and ideally the distribution of sampling points should approximate a normal distribution with the mean (in relative coordinates) approaching zero. Typical time series of the horizontal and vertical velocity components u_i ($i = x, y, z$) corresponding to the east–west, north–south, up–down coordinate axes are shown in Fig. 6. Fig. 7 shows the corresponding velocity correlation functions while the typical power spectrum of velocity time series is shown in Fig. 8, the main events identified with a period of ~3 s (close to the observed wave pattern) corresponding to ~10 ensembles based on a sampling period of 0.39 s. The error reduction resulting from averaging of the time-series using a low-pass filter with a window size corresponding to 10 ensembles is about one-third.

3.2. Autocorrelation function

In Fig. 7, typical results from the numerical computations of the autocorrelation function are presented. For each study and each coordinate axes, the autocorrelation, R_i was computed from the velocity time series using (2). These R_i values compared well with the analytical models from Taylor (1920), Frenkiel (1953), Altinsoy and Tugrul (2002). Care must be taken, however, in applying this close to the boundaries as it was observed that at certain depth cells particularly the bottom layers,

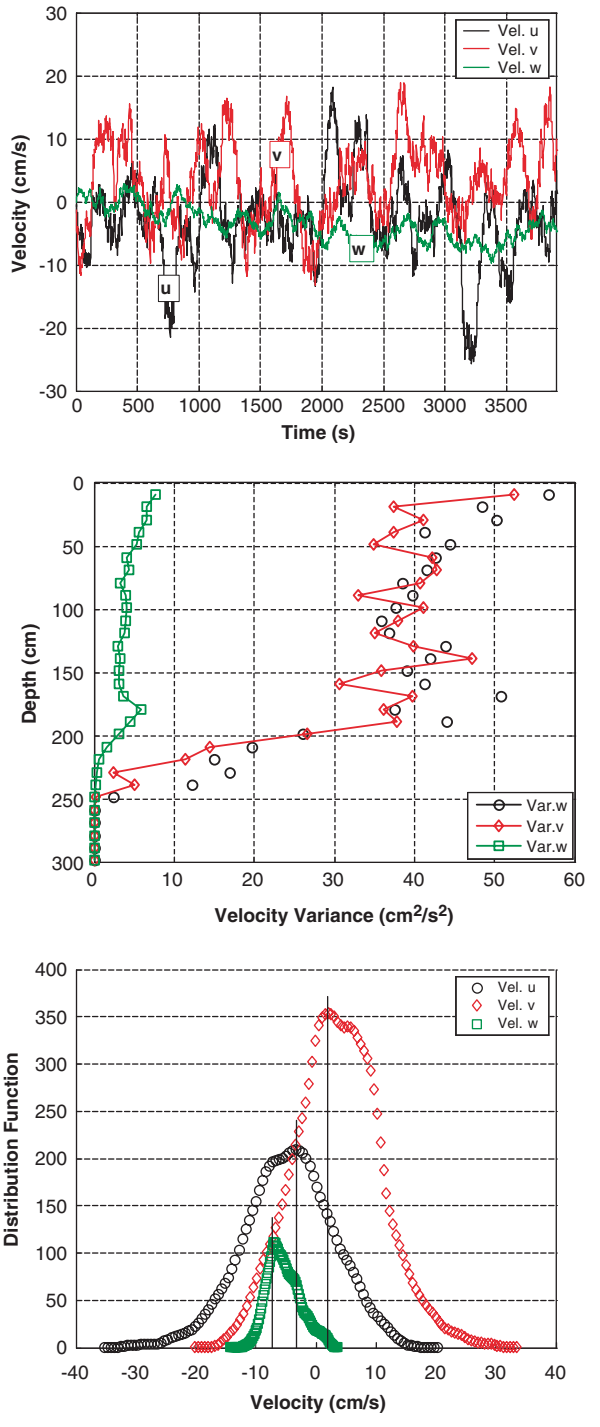

Fig. 6. Top, typical time series of velocity fluctuations along x, y, z coordinate axes, respectively; middle, corresponding depth profile of average velocity variance; bottom, corresponding velocity distribution function.

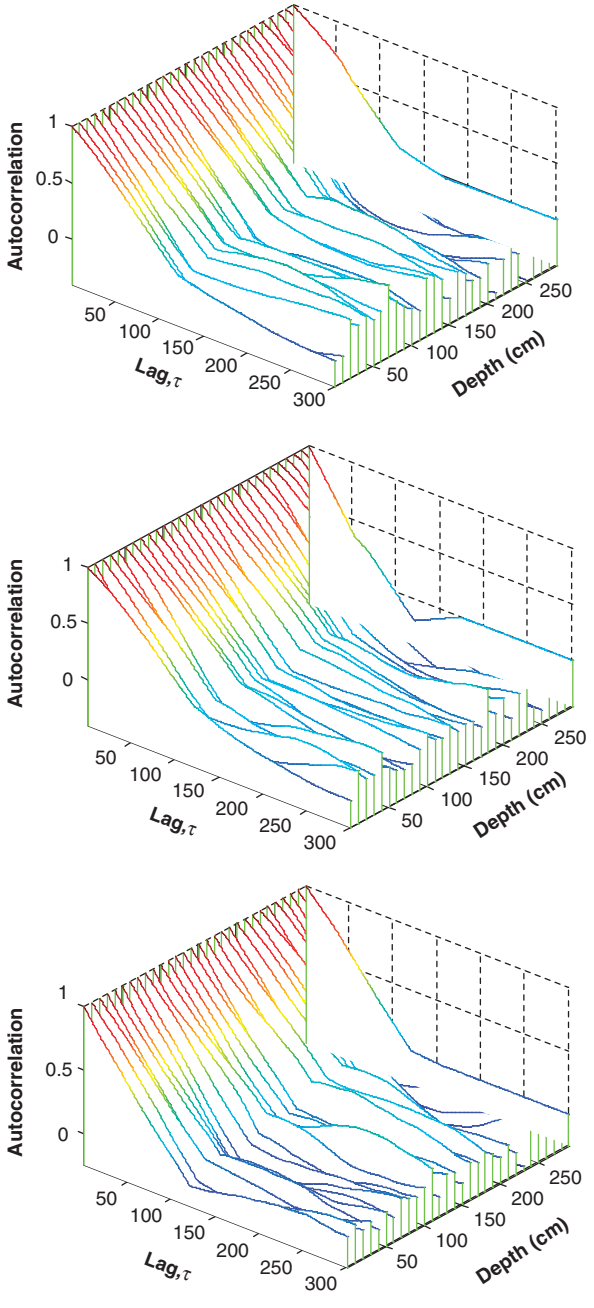

Fig. 7. From top to bottom, velocity autocorrelation function derived from velocity time series along x, y, z coordinate axes, respectively.

the values of R_i became negative which would be seen as a direct violation of its properties as previously outlined. For the most part, R_i was bounded, asymptotically decreasing as prescribed and the results compare with those obtained by Bowden using similar numerical methods.

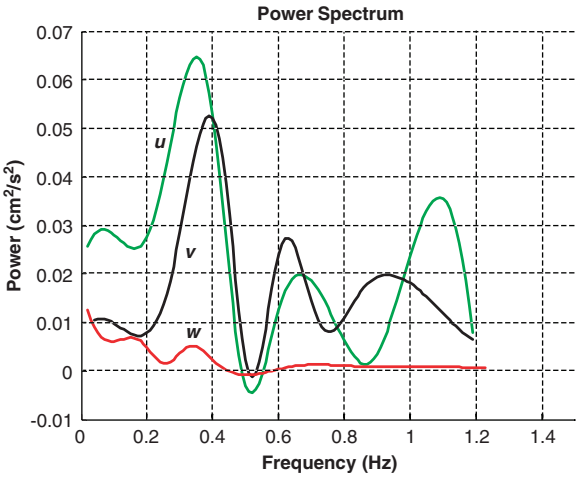

Fig. 8. Typical power spectrum (mean-square) of velocity time series up to the Nyquist frequency. Identified ~3 s period events (corresponding to ~10 ensembles) used in sizing low-pass filter for noise and error reduction.

3.3. Turbulent scale of diffusion and turbulent diffusivity

The Eulerian time scales of turbulence were computed using the integral in Eq. (2). The numerically computed values of the time scale, T_i^E are presented in Table 2. Generally, the values of T_i^E were determined to fall within the range 5–84 s but between the depth cells, the values were found to fall within a relatively narrow range, suggestive of the fact that the turbulence structure does not vary significantly with depth.

An estimate of the spatial extent of diffusing clouds over a given period or diffusion time of ~6000 s was obtained assuming $2\sigma_i$ (68% of distribution) as representative of the spread of the cloud along each coordinate axis. The estimated horizontal spatial extent for study 0828_1 was 220 and 142 m in x, y directions, respectively, giving an aspect ratio of 1.6 for the diffusing patch. For study 0828_2 (Fig. 9), the corresponding values were 226 and 128 m, respectively, with an aspect ratio of 1.8 while the values for study 1007 were found to be 149 and 132 m, respectively, with aspect ratio of 1.1. These values for a cloud in turbulent diffusion were used in providing estimates for $K_i(=\frac{1}{2}d\sigma^2/dt)$ during the different studies (Table 2). From Eq. (3), values for the scaling coefficient, β were in the range 1–3.

The depth profile of the diffusivities along each of the three coordinate axes was numerically computed

Table 2
Summary of turbulent diffusivity results for all three studies conducted

	Time scale of diffusion, T_i^E (s)			Length scale, l_i (cm)			Turbulent diffusivity ($\times 10^4\,cm^2\,s^{-1}$)				Scaling coeff., β
	Mean	Max.	Std. Dev.	Mean	Max.	Std. Dev.	Mean	Max.	Std. Dev.	Observed	
Study 0828_1											
Coordinate axis											
x	25	47	8	284	680	106	0.32	0.98	0.16	1.15	3
y	27	42	9	245	380	94	0.23	0.41	0.10	0.20	2
z	71	84	10	184	260	52	0.05	0.08	0.02	0.00	1
Study 0828_2											
Coordinate axis											
x	28	42	8	337	640	116	0.4	1.03	0.18	1.20	3
y	24	37	8	224	353	77	0.21	0.33	0.08	0.25	2
z	27	40	7	50	79	15	0.01	0.02	0.00	0.00	1
Study 1007											
Coordinate axis											
x	21	34	9	205	387	116	0.22	0.45	0.14	8.00	3
y	19	31	7	157	284	75	0.14	0.35	0.08	2.40	2
z	23	40	8	35	73	18	0.01	0.01	0.00	0.00	1

Mean and maximum values of the diffusivity, integral time and length scales computed during each study for each of the three coordinate axes, *x, y,* The higher observed diffusivity in Study 1007 suggests that shear diffusion may have been the dominant process during this particular study compared to the other two studies.

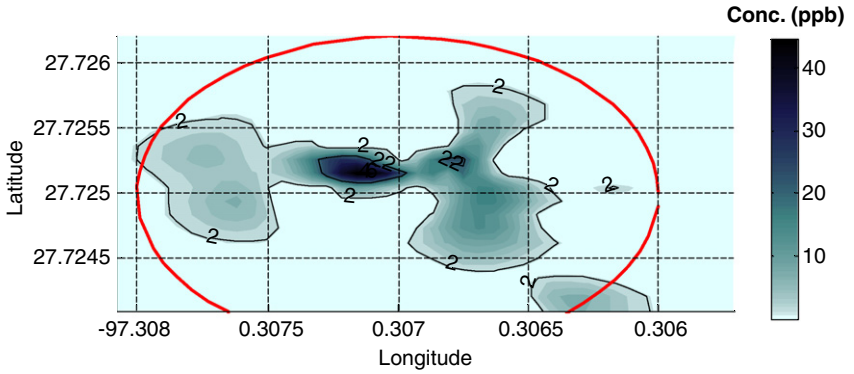

Fig. 9. Observed dye patch from study 0828_2, 6202 s after instantaneous release. Outlined (- - -) is the 68% numerical estimate of spread within 2σ based on computed turbulent parameters ($K_x = 1.03 \times 10^4$, $K_y = 0.33 \times 10^4$).

using Eq. (3) and the results are displayed in Fig. 10. The maximum diffusivity was $1.03 \times 10^4\,cm^2\,s^{-1}$ while the mean turbulent diffusivity was $\sim 0.4 \times 10^4\,cm^2\,s^{-1}$ for the east–west (i.e. 'x') coordinate axis. For the north–south (i.e. 'y') coordinate axis the maximum value was $0.41 \times 10^4\,cm^2\,s^{-1}$, about one order of magnitude less than the values for the east–west axis, while the mean value was $\sim 0.20 \times 10^4\,cm^2\,s^{-1}$. Similarly, the maximum vertical turbulent diffusivity was $0.08 \times 10^4\,cm^2\,s^{-1}$, about two orders of magnitude less than the corresponding values along the x-coordinate and one order of magnitude less than the values along the y-coordinate directions, respectively. These values are summarized in Table 2 and compares well with values obtained for selected bodies of water taken from data found in the literature (Murthy, 1975; Riddle and Lewis, 2000; Ward, 1985).

The time and length scales of turbulent diffusion were found to be within the range expected of oceanographic processes being ~ 100 s and ~ 10 m, respectively. The mean and maximum length scale, l_i for the various depth cells and coordinate axes are

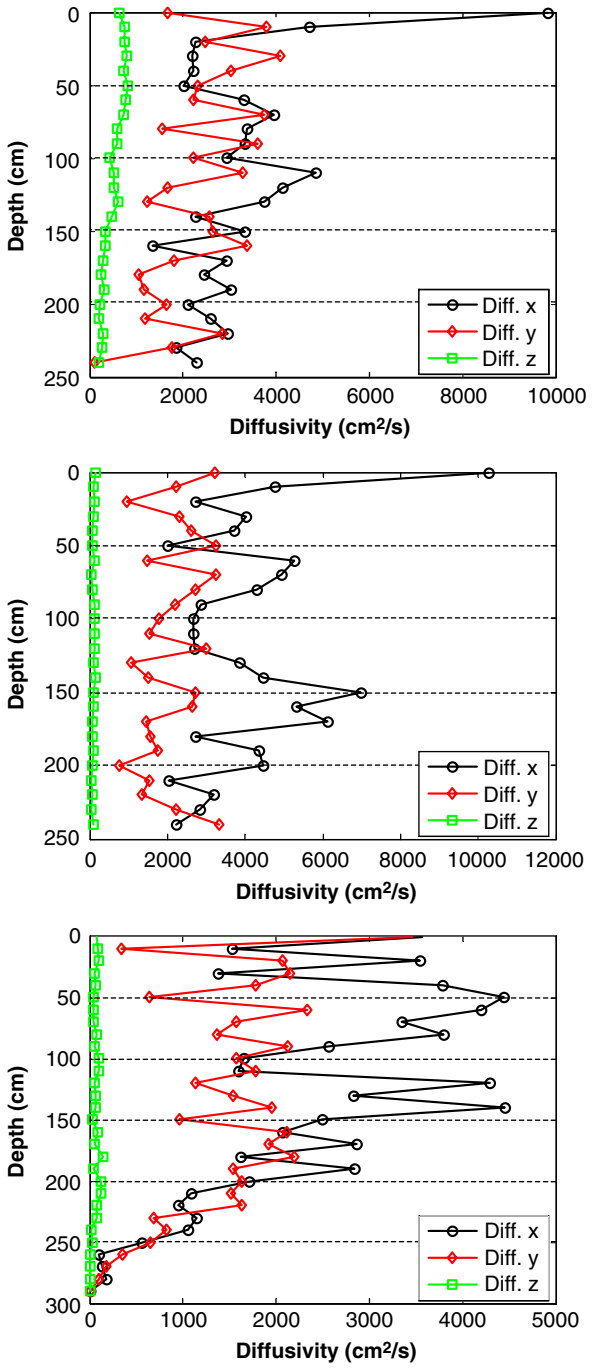

Fig. 10. From top to bottom: depth profile of turbulent diffusivity for each of the three studies. Top, study 0828_1; middle, study 0828_2; bottom, study 1007. Open circle (—○—), x coordinate; diamond (——◇——), y coordinate; open squares (——□——), z coordinate.

presented in Table 2. The length scales range in value from 0 to 680 cm with a significant difference in values between the east–west (mean, 205–337 cm), the north–south (mean, 157–245 cm) and the vertical (mean, 35–184 cm) directions.

4. Discussion

The results of this study are important in the light of episodic events in shallow embayments and the diffusive effects of turbulence occurring within the first few hours following a pulse discharge. Ward had conducted horizontal dye-diffusion experiments under geomorphologic conditions similar to the ones reported in this paper and although no data were reported specifically for Corpus Christi Bay (except the Upper Laguna Madre), the results obtained for horizontal diffusivity values are comparable. Also the values reported by Riddle and Lewis (2000) for bodies of water similar in depth to Corpus Christi Bay show comparable vertical diffusivities to the figures reported in this study. It is pertinent to note that the mean value of the turbulent length scale (~3 m) is comparable to the average depth of the bay which reflects the maximum size of eddies involved in the process. This is to be expected as the size of the turbulent eddies would be limited by the existence of a boundary either physical or virtual, where virtual boundaries may be due to stratification within the water column.

Through this study, the dependence of the turbulence process on the *degree of randomness* as measured through the intensity of turbulence, akin to the dependence of molecular diffusivity on the temperature of the bulk fluid, was examined for Corpus Christi Bay. A numerical algorithm was developed for evaluating diffusivity values from direct observations of the 3D currents field and calibrated against concentration profiles obtained through dye-tracer experiments. The resulting turbulent diffusivities compared well with those obtained using oceanic diffusion diagrams. The study was limited in terms of spatial and temporal scales in order to filter out the gross effects of tidal and inertial motion on the diffusion process. Future studies will allow the extension of this concept to the entire bay premised on the availability of surface current mapping data to coincide with the turbulent processes that drive constituent transport on the scale of days to months.

For study 1007, although the turbulent diffusivity values (hence the computed spatial extent) were much lower than the values from the other two experiments, actual dye patch observations

(Table 2) were much higher and may be indicative of the onset of shear diffusion. This shear diffusive process has been observed in pipe and channel flows by several researchers (Csanady, 1966; Elder, 1958; Elliot, 1986; Taylor, 1954) and will be the subject of future studies along with the dependence of the scaling coefficient on turbulence intensity and water column stability.

5. Conclusion

The ability to characterize diffusion processes from hydrodynamic information is important as it can be applied to different bodies of water especially when viewed against the backdrop of the logistical challenge and expense associated with conducting dye-tracer experiments. As was determined from this study, the process of diffusion in surface waters particularly wind-driven bays such as Corpus Christi Bay is not always shear-dominant but depending on prevailing conditions, may be dominated by pure turbulence. This is significant against the backdrop of general and ocean circulation models that employ turbulence closure schemes premised on the assumption of shear-diffusion. The algorithm developed in this study was calibrated against observed spread of a dye patch, and will allow for the inclusion of diffusivity values within the framework of a data-driven transport model using direct hydrodynamic observations. This would form a logical extension of existing oceanographic instrumentation to environmental assessments and precludes the application of turbulence closure schemes that base estimates of diffusivity on the assumption of prevailing shear.

Although this study does not answer all the questions regarding the enigma of turbulence, observations from these set of experiments contributes to the data on diffusion processes available for coastal and nearshore environments with emphasis on Corpus Christi Bay, data that are usually not found through the use of available oceanic diffusion diagrams. Considering that current profilers of the type used in this study are readily available, more experiments of this type can be conducted in a cost effective manner and this study establishes the methodology for such experiments with a view to better characterize the diffusive process within the study area. Future work will investigate the shear-diffusion process for Corpus Christi Bay with a view to developing similar algorithm necessary for evaluation of shear-diffusivity values from observed hydrodynamic data. These algorithms will be applied within a data-driven transport model that is part of the ongoing development process within our laboratory.

Acknowledgements

This work was funded in part by funds from Texas Higher Education Coordinating Board (THECB-TDT 011161-0011-2001) and by funds from National Science Foundation (NSR-MRI C02-00533). Special thanks go to the Texas general land office (TGLO) in providing support for this project. The authors would like to thank the research staff at the Shoreline Environmental Research Facility at Texas A and M University for helping with the data collection.

References

Altinsoy, N., Tugrul, A.B., 2002. A new proposal for Lagrangian correlation coefficient. International Journal of Heat and Fluid Flow 23, 766–768.

Barrick, D.E., Headrick, J.M., Bogle, R.W., Crombie, D.D., 1977. Ocean surface currents mapped by radar. Science 198, 138–144.

Bowden, K.F., Fairbairn, L.A., 1952. Further observations of the turbulent fluctuations in a tidal current. Philosophical transactions of the Royal Society of London. Series A, Mathematical and Physical Sciences 244, 335–356.

Bowden, K.F., Howe, M.R., 1963. Observations of turbulence in a tidal current. Journal of Fluid Mechanics 17, 271–284.

Csanady, G.T., 1966. Accelerated diffusion in the skewed shear flow of lake current. Journal of Geophysical Research 71, 411–420.

Elder, J.W., 1958. The dispersion of marked fluid in turbulent shear flow. Journal of Fluid Mechanics 8, 33–40.

Elliot, A.J., 1986. Shear diffusion and the spread of oil in the surface layers of the North Sea. Dt. Hydrology Z. 39, 114–137.

Ernest, A.N., Bonner, J.S., Autenrieth, R.L., 1991. Model parameter-estimation for particle-transport. Journal of Environmental Engineering-ASCE 117, 573–594.

Fischer, H.B., List, E.J., Koh, R.C.Y., Imberger, J., Brooks, N.H., 1979. Mixing in Inland and Coastal Waters. Academic Press, San Diego, 483pp.

Frenkiel, F.N., 1953. Turbulent Diffusion: Mean concentration distribution in a flow field of homogeneous turbulence. In Advanced Applied Mechanics, 3: New York, Academic Press, pp. 61–107.

Hanna, S.R., 1981. Lagrangian and Eulerian time-scale relations in the daytime boundary layer. Journal of Applied Meteorology 20, 242–249.

Hay, J.S., Pasquill, F., 1959. Diffusion from a continuous source in relation to the spectrum and scale of turbulence. Advances in Geophysics 6, 345.

Kelly, F.J., Bonner, J.S., Ojo, T.O., Durel, A., 2004. Port Freeport's "FlowInfo": An example of an Integrated Port Navigation and Environmental Data System (IPNEDS). ASCE Ports 2004 Conference.

Kelly, F.J., Bonner, J.S., Perez, J.C., Adams, J.S., Prouty, D.B., Trujillo, D., Weisberg, R.H., Luther, M.E., He, R., Cole, R., Donovan, J., Merz, C.R., 2002. An HF Radar Test Deployment Amidst an ADCP Array on the West Florida Shelf. Sixth Working Conference on Current Measurement Technology, pp. 692–698.

Lee, D.G., Bonner, J.S., Garton, L.S., Ernest, A.N., Autenrieth, R.L., 2000. Modeling coagulation kinetics incorporating fractal theories: a fractal rectilinear approach. Water Research 37, 1987–2000.

Murthy, C.R., 1975. Horizontal diffusion characteristics in Lake Ontario. Journal of Geophysical Research 6, 76–84.

O'Connor, T.P., Walker, H.A., Paul, J.F., Victor J. Bierman, J., 1985. A strategy for monitoring of contaminant distributions resulting from proposed sewage sludge disposal at the 106-mile ocean disposal site. Marine Environmental Research 16, 127–150.

Ojo, T., Bonner, J., 2002. 3-Dimensional Self-Calibrating Coastal Oil Spill Trajectory Tracking and Contaminant Transport using HF Radar. In: Proceedings of the 25th Arctic and Marine Oilspill Program (AMOP) Technical Seminar, pp. 215–226.

Ojo, T., Bonner, J., Fuller, C., Kelly, F., Page, C., Sterling, M.J., 2003a. Field Simulation of Aerial Dispersant Application for Spill of Opportunity. In: Proceedings of the 26th Arctic and Marine Oilspill Program (AMOP) Technical Seminar, these proceedings, pp. 813–824.

Ojo, T., Sterling, M.C.J., Bonner, J.S., Fuller, C.B., Kelly, F., Page, C.A., 2003b. Multi-parameter instrument array and control system (MPIACS): a Software interface implementation of real-time data acquisition and visualization for environmental monitoring. MTS/IEEE Oceans 2003 Conference.

Ojo, T.O., Bonner, J.S., Sterling, M.C., Fuller, C.B., Page, C.A., Autenrieth, R.L., 2003c. Implementation of Distributed Computing System for Emergency Response and Contaminant Spill Monitoring. Twenty-sixth Arctic and Marine Oilspill Program (AMOP) Technical Seminar, pp. 287–297.

Okubo, A., 1971. Oceanic diffusion diagrams. Deep-Sea Research 18, 789–802.

Paul, J.F., Victor, J., Bierman, J., Walker, H.A., Gentle, J.H. (Eds.), 1989. Application of a Hazard-Assessment Research Strategy for Waste Disposal at 106-Mile Ocean Disposal Site: Oceanic Processes In Marine Pollution, vol. 4. Robert E. Krieger Publishing Company, Malabar, Florida, 286pp.

Riddle, A.M., Lewis, R.E., 2000. Dispersion experiments in UK coastal waters. Estuarine, Coastal and Shelf Science 51, 243–254.

Schott, F., 1978. Langrangian and Eulerian measurements of horizontal mixing in the Baltic. Tellus 31, 139–143.

Sterling, J., Michael, C., Bonner, J.S., Ernest, A.N.S., Page, C.A., Autenrieth, R.L., 2004a. Characterizing aquatic sediment-oil aggregates using *in situ* instruments. Marine Pollution Bulletin 48, 533–542.

Sterling Jr., M.C., Bonner, J.S., Page, C.A., Fuller, C.B., Ernest, A.N., Autenrieth, R.L., 2004b. Modeling crude oil droplet-sediment aggregation in nearshore waters. Environmental Science and Technology 38, 4627–4634.

Taylor, G.I., 1920. Diffusion by continuous movements. Proceedings of the London Mathematical Society 20, 196–211.

Taylor, G.I., 1938. The spectrum of turbulence. Proceedings of the Royal Society of London Series A 164 (919), 476–490.

Taylor, G.I., 1954. The dispersion of matter in Turbulent flow through a pipe. In: Proceedings of the Royal Society of London Series A, 446–467.

Ward, G.H., 1985. Dye diffusion experience in the Texas bays; low-wave conditions. Journal of Geophysical Research 90, 4959–4968.